RSC Advances

PAPER

View Article Online
View Journal | View Issue

Cite this: *RSC Adv.*, 2021, **11**, 1564

Fullerene–porphyrin hybrid nanoparticles that generate activated oxygen by photoirradiation†

Kouta Sugikawa,* Kosuke Masuda, Kentaro Kozawa, Riku Kawasaki and Atsushi Ikeda*

Received 4th November 2020
Accepted 2nd December 2020

DOI: 10.1039/d0ra09387d

rsc.li/rsc-advances

The preparation of water-dispersible hybrid nanoparticles comprising fullerene and porphyrin from cyclodextrin complexes is described. In the presence of polyethylene glycol, C_{60} fullerene and porphyrin were expelled from the cyclodextrin cavity to form fullerene–porphyrin hybrid nanoparticles in water. The fullerene–porphyrin hybrid nanoparticles exhibit improved singlet oxygen generation ability under photoirradiation compared with that of C_{60} nanoparticles.

Water-dispersible colloidal fullerene assemblies, referred to as fullerene nanoparticles (NPs), have recently received increasing attention.[1–3] Fullerene NPs are negatively charged and can be dispersed in water in the absence of any solubilizer. Fullerene NPs demonstrate promise within biological and medical applications, as radical scavengers and photosensitizers for photodynamic therapy. To further extend the applications of fullerene NPs, additional hybridization with desired functional molecules is required. Porphyrin and associated derivatives are highly promising candidates for hybridization with fullerenes to increase photoactivity.[4] Numerous studies on the complexation of fullerenes with porphyrin molecules using synthetic organic chemistry[5–7] or supramolecular chemistry[8–10] have been reported. Although fullerene NPs have been intensively studied over the last decade, no reliable method to achieve the hybridization of porphyrins with fullerene NPs has been proposed.

Poly(ethylene glycol) monomethyl ether (PEG) was recently observed to accelerate the decomposition of fullerene C_{60}–γ-CD complexes in water, which leads to the rapid aggregation of C_{60} to form water-dispersible C_{60} NPs.[11] In this method, C_{60}–γ-CD complexes can exist as stable isolated molecules in water, enabling the precise size control and step-wise growth of C_{60} NPs.[12,13] Herein, the preparation of hybrid NPs comprising C_{60} and hydrophobic porphyrin molecules are reported. C_{60}–γ-CD and porphyrin-trimethyl-β-cyclodextrin (por–TMe-β-CD) complexes are mixed in water in the presence of PEG. Both complexes decompose through the interaction of PEG with the CDs, leading to the formation of C_{60}–porphyrin hybrid NPs (denoted as C_{60}–por NPs). The C_{60}–por NPs are negatively charged and easily disperse in water. Additionally, the ability of C_{60}–por NPs to generate activated oxygen is also evaluated.

The C_{60}–γ-CD complex[14,15] and **1**–TMe-β-CD complex (Fig. 1)[16–18] were prepared according to a previously described procedure (see the ESI† for details). The ^{1}H NMR spectrum of the mixed solution comprising the C_{60}–γ-CD complex and PEG after 1 h incubation at 80 °C shows that the peaks attributed to the C_{60}–γ-CD complexes completely disappeared (Fig. S1†). Hence, the ^{1}H NMR data confirm the decomposition of the C_{60}–γ-CD complexes and the formation of water-dispersible C_{60} NPs, as previously reported.[11–13] The effect of PEG on **1**–TMe-β-CD complexes was also investigated by ^{1}H-NMR as shown in Fig. S2.† After incubating the mixed solution of **1**–TMe-β-CD complex and PEG ([**1**] = 0.1 mM, [PEG] = 5.0 g L^{-1}) for 1 h at room temperature, peaks attributed to the **1**–TMe-β-CD complex were still evident at 4.97 ppm and above 7.7 ppm (Fig. S2(i)†). Hence, PEG has no influence upon the **1**–TMe-β-CD structure at room temperature. Conversely, after incubating for 1 h at 80 °C, a dark purple precipitate formed and the aforementioned ^{1}H NMR peaks completely disappeared (Fig. S2(ii)†). In the absence of PEG, the **1**–TMe-β-CD complex was stable in water both at room temperature (Fig. S2(iii)†) and 80 °C (Fig. S2(iv)†). These results suggest a decomposition route of **1**–TMe-β-CD by interaction with PEG at 80 °C, with a concomitant formation of non-dispersible large aggregates.

To obtain hybrid NPs comprising C_{60} and **1** (C_{60}–**1** NPs), PEG (M_w = 2000) was added to an aqueous solution containing C_{60}–

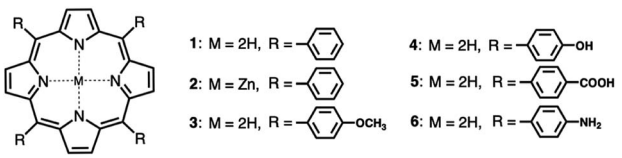

Fig. 1 Chemical structures of porphyrin derivatives used in this study.

Applied Chemistry Program, Graduate School of Advanced Science and Engineering, Hiroshima University, Higashi-Hiroshima 739-8527, Japan. E-mail: sugikawa@hiroshima-u.ac.jp; aikeda@hiroshima-u.ac.jp

† Electronic supplementary information (ESI) available: Experimental details and Fig. S1–S6. See DOI: 10.1039/d0ra09387d

γ-CD and **1**–TMe-β-CD complexes ([C_{60}] = [**1**] = 0.1 mM, [PEG] = 5.0 g L^{-1}), which were thereafter incubated at room temperature or 80 °C. The ^{1}H NMR spectrum of the mixed solution at room temperature shows peaks attributed to γ-CD in the C_{60}–γ-CD complex at 5.03 ppm, TMe-β-CD in the **1**–TMe-β-CD complex at 4.97 ppm, and **1** in the **1**–TMe-β-CD complex in the region of 7.6–8.5 ppm (Fig. 2a(i)). The data indicate that PEG fails to induce the decomposition of the C_{60}–γ-CD and **1**–TMe-β-CD complexes at room temperature. Conversely, after the mixture was heated at 80 °C for 1 h, the peaks attributed to the C_{60}–γ-CD and **1**–TMe-β-CD complexes completely disappeared (Fig. 2a(ii)). Hence, C_{60}–γ-CD and **1**–TMe-β-CD were decomposed at 80 °C, in the presence of PEG. The solution after being subjected to heat treatment at 80 °C for 1 h, was dark purple in the absence of any precipitate. The hydrodynamic diameter and ζ-potential of the reacted solution were 125 nm (polydispersity index = 0.21) and −20.2 mV, respectively. Water dispersible fullerene NPs typically exhibit negative ζ-potentials, the origin of which still requires elucidating.[19,20] Hence, the formation of water-dispersible nano-composites, C_{60}–**1** NPs, is suggested.

The por–TMe-β-CD complexes using **2**–**6** (Fig. 1), were also prepared adopting the same procedure as that for the **1**–TMe-β-CD complex. Each por–TMe-β-CD complex solution was mixed with C_{60}–γ-CD and PEG ([C_{60}] = [por] = 0.1 mM, [PEG] = 5.0 g L^{-1}). The ^{1}H NMR spectrum of each individual mixed solution after being incubated for 1 h at 80 °C, is shown in Fig. S3.† In the ^{1}H NMR spectrum of the mixture comprising C_{60}–γ-CD and **2**–TMe-β-CD, the peaks attributed to these complexes at 5.03, 4.98, and 7.60–8.50 ppm, completely disappeared after being subjected to incubation for 1 h at 80 °C, without precipitation (Fig. S3a†). Similar changes in the ^{1}H NMR spectrum of the mixture comprising C_{60}–γ-CD and **3**–TMe-β-CD complexes are observed, as shown in Fig. S3b.† The data suggest that the **2**–TMe-β-CD and **3**–TMe-β-CD complexes can be decomposed in a similar manner as the C_{60}–γ-CD complexes, and imply the formation of C_{60}–**2** and C_{60}–**3** NPs.

The ^{1}H NMR spectra of the mixed solutions comprising C_{60}–γ-CD and **4**, **5**, or **6**–TMe-β-CD complexes failed to show peaks attributed to the C_{60}–γ-CD complex, and peaks associated with the respective por–TMe-β-CD complexes were observed after incubation for 1 h at 80 °C (Fig. S3c–e,† respectively). Hence, the data suggest that the C_{60}–γ-CD complex decomposed in the presence of PEG, and the **4**, **5**, and **6**–TMe-β-CD complexes were observed to be stable without decomposition at 80 °C. There have been reports suggesting the strong interaction of water-soluble tetraphenyl porphyrins with TMe-β-CDs.[21,22] Polar substituents prompt the penetration of the polarized porphyrin rims into the TMe-β-CD cavity. Porphyrins **4**–**6** possess polar substituents, which are suggested to enable the formation of stable TMe-β-CD complexes. Furthermore, the size of the β-CD cavity is sufficiently narrow to prevent any strong interaction with PEG.[23] Thus, PEG-induced decomposition of the **4**, **5**, and **6**–TMe-β-CD complexes is not possible.

The absorption behavior of C_{60}–**1** NPs was investigated using ultraviolet-visible (UV/Vis) spectroscopy. In the UV/Vis spectra, the characteristic peak of solvated C_{60}–γ-CD, at 333 nm shifted to 344 nm after heating at 80 °C for 1 h (Fig. 2b). An additional broad absorption at 400–550 nm is also apparent, which is characteristic of solid-state crystalline C_{60} and arises from the electronic interactions between adjacent C_{60} molecules.[24,25] The characteristic peak of the solvated **1**–TMe-β-CD complex at 415 nm, shifted to 432 nm, with induced broadening after being subjected to heat treatment at 80 °C for 1 h (Fig. 2b). In the absence of C_{60}–γ-CD complexes, the characteristic absorption peak attributed to the solvated **1**–TMe-β-CD complex completely disappeared after heating for 1 h at 80 °C, in the presence of PEG (Fig. S4†). The data show that **1**, when expelled from the TMe-β-CD cavities, forms non-dispersible precipitates in the absence of C_{60}. For **1** dispelled from the TMe-β-CD cavities to be stably dispersed in water, formation of co-aggregates with C_{60} may be a prerequisite. C_{60}–**2** and C_{60}–**3** NPs also show similar UV-Vis absorption spectra after being subjected to heating at 80 °C for 1 h, as shown in Fig. S5a and b,† respectively.

To further elucidate the composite formation of C_{60} and **1**, the influence of **1** concentration on C_{60}–**1** NP formation was investigated by UV/Vis spectroscopy (Fig. 2c). The intensity of the absorption peak at 432 nm increased as a function of **1** concentration from 0.05 to 0.1 mM. Conversely, the absorption peak at 345 nm, derived from the formation of fullerene NPs, shifted to 338 nm, with increasing concentration of **1**. This absorption peak derives from the fullerene nanoparticle size, and as the size decreased (*i.e.*, the NPs became smaller), the

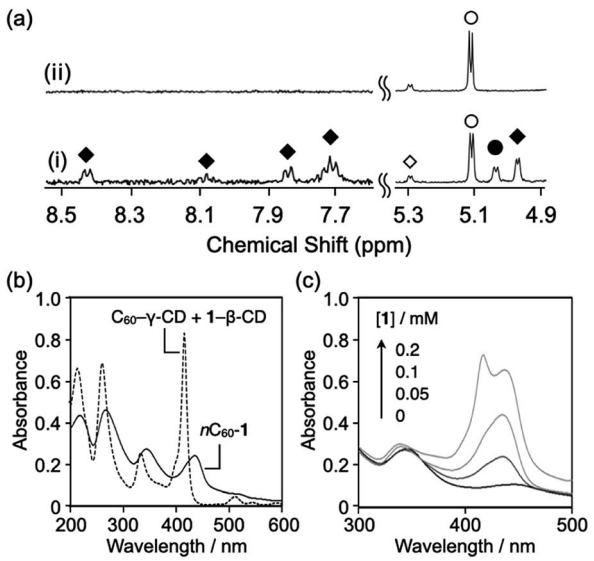

Fig. 2 (a) ^{1}H NMR spectra of mixed solutions comprising fullerene C_{60}–γ-cyclodextrin (CD) and **1**–trimethyl (TMe)-β-CD complexes ([C_{60}] = [**1**] = 0.1 mM) (i) before and (ii) after heating at 80 °C for 1 h, in the presence of polyethylene glycol (PEG) (5 g L^{-1}). Open circles: free γ-CD, filled circles: C_{60}–γ-CD, open diamonds: free TMe-β-CD, and filled diamonds: porphyrin–TMe-β-CD (por–TMe-β-CD) complex. The spectra at 7.6–8.5 ppm, are amplified five-fold. (b) Ultraviolet-visible (UV/Vis) absorption spectra of the mixed solution comprising C_{60}–γ-CD and **1**–TMe-β-CD complexes ([C_{60}] = [**1**] = 0.1 mM) with PEG (5 g L^{-1}), before (dashed line) and after (solid line) heating at 80 °C for 1 h. (c) UV/Vis absorption spectra of the mixed solution comprising the C_{60}–γ-CD complex as a function of the **1**–TMe-β-CD complex concentration ([C_{60}] = 0.1 mM, [**1**] = 0–0.2 mM) with PEG (5 g L^{-1}) after heating at 80 °C for 1 h.

peak blue-shifted.[11] The results suggest that in the presence of **1**, the fullerene interaction might be disturbed, or smaller C_{60} NPs might form. For C_{60}–**1** NPs formulated with 0.2 mM of **1** ([C_{60}] = 0.1 mM, [**1**] = 0.2 mM), the absorption peak derived from the Soret band of **1** split into two peaks (Fig. 2c). The absorption peak at the shorter wavelength of 415 nm is consistent with that of the **1**–TMe-β-CD complex. The absorption peak at the longer wavelength of 431 nm is almost consistent with the absorption peaks in the UV/Vis spectra of C_{60}–**1** NPs fabricated with 0.05 and 0.1 mM of **1**. The findings indicate that in the sample comprising 0.2 mM of **1**, a portion of the **1**–TMe-β-CD complexes remained in the complex state after heating for 1 h at 80 °C, in the presence of PEG. The absorption peak at 338 nm, which reflects the state of fullerene NPs, is similar to that of C_{60}–**1** NPs fabricated with 0.1 mM of **1**. When C_{60} and **1** form co-aggregated NPs, the ratio of **1** to C_{60} is thought to be limited to ~1 : 1.

Morphological observations of the hybrid NPs were also undertaken. In the absence of the por–TMe-β-CD complex, C_{60} NPs possessing fairly monodisperse size distributions were observed (Fig. S6a†). The average diameter of the individual NPs, determined from the transmission electron microscopy (TEM) images, is 82 nm. C_{60} NPs have been previously reported to exhibit lattice fringes and diffraction patterns, which suggests that C_{60} NPs maintain the face-centered cubic (fcc) crystalline structure.[11] C_{60}–**1** NPs prepared with 0.05 mM C_{60} and 0.1 mM **1**, possessed irregular shapes (Fig. 3a and b, respectively). The average diameter of C_{60}–**1** NPs, determined by TEM, is 119 nm (Fig. 3a and S6b†), demonstrating the larger C_{60}–**1** NP size than that of the C_{60} NPs (82 nm). Increasing the concentration of **1** to 0.1 mM results in the average diameter of C_{60}–**1** NPs to increase to 131 nm (Fig. 3b and S6c†). Similar morphology is observed from the TEM micrographs of C_{60}–**2** and C_{60}–**3** NPs having average diameters of 109 nm and 144 nm, respectively (Fig. 3c and d, respectively). A lower PEG molecular weight or a lower reaction temperature during C_{60} NP formation *via* C_{60}–γ-CD complexes have been reported to induce an increase in the diameter of the C_{60} NPs.[11,12] Thus, the findings suggest that slower reaction conditions result in less nucleation and a larger NP formation. Porphyrin **3** possesses a methoxy substituent at the *para* position of the phenyl group and is more polar than **1** or **2**. Previous reports have demonstrated that the higher the polarity of the phenyl group, the more stable the complex with TMe-β-CD,[21,22] which indicates that **3**–TMe-β-CD is more stable than **1**– or **2**–TMe-β-CD in water. Thus, the aforementioned decomposition, which results from the interaction with PEG, is slower in **3** with a concomitant increase in the NP size.

In the high-resolution TEM micrograph (Fig. 3e), the C_{60}–**1** NPs only exhibited partial lattice fringes, and hence did not show clear diffraction patterns compared with the C_{60} NPs (inset in Fig. 3e).[11] The findings demonstrate the highly amorphous nature of the C_{60}–**1** NPs, and that the C_{60} crystal structure was only retained in part. ^{13}C NMR spectra also provide important information about the structure of the C_{60}–**1** NPs. A characteristic C_{60} cluster signal at 142.4 ppm was detected in both C_{60} NPs and C_{60}–**1** NPs (Fig. 3f).[26] The C_{60}–**1** NP dispersions also exhibited several small new signals at 141.5, 143.3, and 143.7 ppm, as shown in Fig. 3f(ii). When a fullerene and a porphyrin molecule form a stable complex in solution, the C_{60} signal shifts depending on the interaction type between the fullerene and the porphyrin molecule.[27] Thus, the porphyrin molecule interacted with the aggregate of C_{60} in C_{60}–**1**, as illustrated in Fig. 3g.

Some porphyrin molecules can form a co-crystal with fullerene C_{60}.[28] To form a crystal structure, not only the interaction between molecules but also the relationship with the solvent, such as gradually changing the polarity of the solvent or removing the solvent, are important. In our system, porphyrin molecules that are pseudo-dissolved by TMe-β-CDs are added to water, which is a poor solvent for porphyrins, through the interaction of PEG with TMe-β-CDs. The porphyrin molecule should immediately aggregate and have difficulty forming a crystal structure. Furthermore, because water is also a poor solvent for fullerene C_{60}, C_{60} also immediately aggregates in water. Thus, it should be extremely difficult for C_{60} and porphyrin molecules to regularly associate to form a co-crystal structure.

The concentration of singlet oxygen molecules ($^1O_2$, Type-II energy transfer pathway) generated by photoirradiation was measured according to a chemical method using 9,10-anthracenediyl-bis(methylene) dimalonic acid (ABDA)[15,29] as a marker to determine the biological activities of C_{60} NPs, C_{60}–**1** NPs, C_{60}–**2** NPs, and C_{60}–**3** NPs. The absorption of ABDA at the absorption maximum (380 nm) was monitored as a function of irradiation time ([C_{60}] = 0.1 mM, [por] = 0 or 0.1 mM). Under visible-light irradiation at wavelengths > 620 nm, C_{60}–**1**

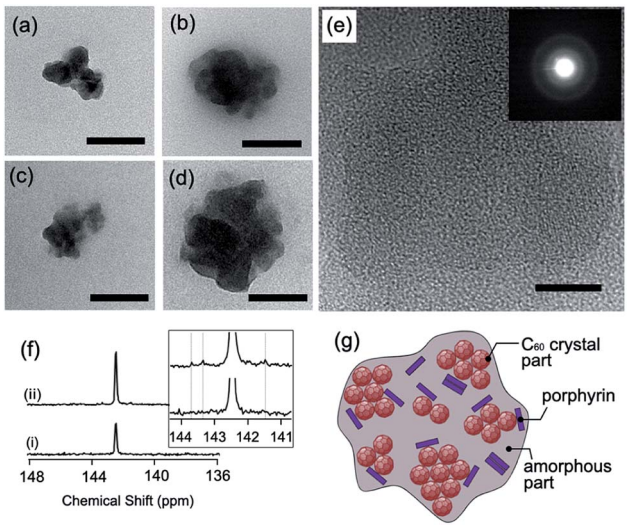

Fig. 3 Transmission electron microscopy (TEM) images of C_{60}–**1** nanoparticles (NPs) prepared with (a) 0.05 and (b) 0.1 mM of the **1**–TMe-β-CD complex. TEM images of (c) C_{60}–**2** and (d) C_{60}–**3** NPs. Scale bars in images (a–d) are 100 nm. (e) High resolution TEM micrograph and selected-area electron diffraction pattern of C_{60}–**1** NP. Scale bar is 10 nm. (f) ^{13}C NMR spectra of (i) C_{60} NPs and (ii) C_{60}–**1** NPs. (g) Illustration of a C_{60}–por NP. A portion of C_{60} form crystalline structures, while a portion of the porphyrin molecules interact with C_{60} at the molecular level.

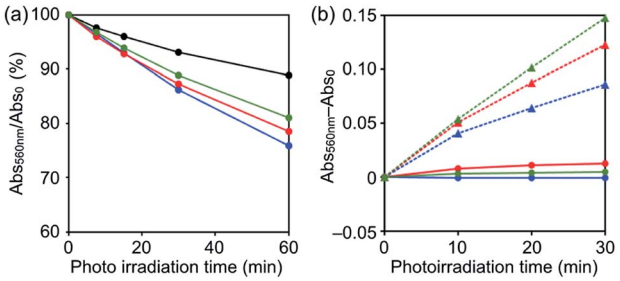

Fig. 4 (a) $^1O_2$ generation by NPs. Bleaching of 9,10-anthracenediyl-bis(methylene) dimalonic acid (ABDA) was monitored as a function of the decrease in the absorbance at 380 nm, for C_{60} NPs (black circles and solid line), C_{60}–**1** NPs (red circles and solid line), C_{60}–**2** NPs (blue circles and solid line), and C_{60}–**3** NPs (green circles and solid line) ([C_{60}] = 15 μM, [por] = 0 or 15 μM, [ABDA] = 25 μM). (b) $O_2^{\bullet-}$ generation by NPs. The amount of formazan generated by the reduction of nitroblue tetrazolium (NBT) in the presence of $O_2^{\bullet-}$ was analyzed by the absorbance at 560 nm, of C_{60}–**1** NPs (red circles) and C_{60}–**2** NPs (blue circles) in the absence (solid lines) and presence (dashed lines) of NADH ([C_{60}] = 15 μM, [por] = 15 μM, [NBT] = 200 μM, [NADH] = 0 or 625 μM). All samples were photoirradiated at >620 nm, in O_2-saturated aqueous solutions.

NPs, C_{60}–**2** NPs, and C_{60}–**3** NPs generated higher levels of $^1O_2$ than C_{60} (Fig. 4a). These results show that the $^1O_2$ photoproduction abilities of the C_{60}–por NPs were higher than that of the C_{60} NPs. There are no significant differences in the $^1O_2$ photoproduction abilities of C_{60}–**1** NPs, C_{60}–**2** NPs, and C_{60}–**3** NPs, which suggests that the structure of the porphyrin has an insignificant influence on the ability of the hybrid NPs. The generation of formazan, *via* the reduction of nitroblue tetrazolium (NBT) by oxygen radicals ($O_2^{\bullet-}$), is observed as an increase of absorption intensity at 560 nm.[30] The reduction of NBT by $O_2^{\bullet-}$ was scarcely detected in solutions containing C_{60}–**1** NPs, C_{60}–**2** NPs, and C_{60}–**3** NPs under photoirradiation, even though formazan was readily detected in the positive control sample in the presence of reduced nicotinamide adenine dinucleotide (NADH) (Fig. 4b). The results suggest that the reactive oxygen species produced by C_{60}–**1** NPs, C_{60}–**2** NPs, and C_{60}–**3** NPs are predominantly $^1O_2$ generated by a Type-II reaction.[18]

In summary, the preparation of hybrid C_{60}–porphyrin NPs was achieved *via* a guest exchange reaction comprising porphyrin CD complexes and C_{60}. Seven C_{60}–por NP derivatives with various moieties were prepared. CD porphyrin complexes possessing phenyl and methoxyphenyl moieties were decomposed in the presence of PEG at the same time as C_{60}–γ-CD complexes and formed NPs with C_{60}. Porphyrins containing a hydrophilic moiety form stable complexes with TMe-β-CD and fail to co-aggregate with C_{60}. The C_{60}–por NPs are negatively charged and are easily dispersed and stable in water. The $^1O_2$ generation ability of C_{60}–por NPs under photoirradiation (>620 nm) is greater than that of C_{60} NPs. The findings herein demonstrate a new method to fabricate fullerene–porphyrin composite materials, which provides a route to highly functional fullerene-based materials.

Conflicts of interest

The authors declare no conflicts of interests.

Acknowledgements

This work was supported by the Japan Society for the Promotion of Science, KAKENHI (Grant No. JP16H04133 and JP19K15523).

Notes and references

1 G. V. Andrievsky, V. K. Klochkov, A. B. Bordyuh and G. I. Dovbeshko, *Chem. Phys. Lett.*, 2002, **364**, 8–17.
2 K. J. Moor, S. D. Snow and J. H. Kim, *Environ. Sci. Technol.*, 2015, **49**, 5990–5998.
3 N. O. McHedlov-Petrossyan, *Chem. Rev.*, 2013, **113**, 5149–5193.
4 D. M. Guldi, *Chem. Soc. Rev.*, 2002, **31**, 22–36.
5 H. Imahori, K. Tamaki, D. M. Guldi, C. P. Luo, M. Fujitsuka, O. Ito, Y. Sakata and S. Fukuzumi, *J. Am. Chem. Soc.*, 2001, **123**, 2607–2617.
6 C. O. Obondi, G. N. Lim and F. D'Souza, *J. Phys. Chem. C*, 2015, **119**, 176–185.
7 S. M. Rezayat, S. V. S. Boushehri, B. Salmanian, A. H. Omidvari, S. Tarighat, S. Esmaeili, S. Sarkar, N. Amirshahi, R. N. Alyautdin, M. A. Orlova, I. V. Trushkov, A. L. Buchachenko, K. C. Liu and D. A. Kuznetsov, *Eur. J. Med. Chem.*, 2009, **44**, 1554–1569.
8 M. Ayabe, A. Ikeda, Y. Kubo, M. Takeuchi and S. Shinkai, *Angew. Chem., Int. Ed.*, 2002, **41**, 2790–2792.
9 P. D. W. Boyd and C. A. Reed, *Acc. Chem. Res.*, 2005, **38**, 235–242.
10 F. D'Souza and O. Ito, *Coord. Chem. Rev.*, 2005, **249**, 1410–1422.
11 K. Sugikawa, K. Kozawa, M. Ueda and A. Ikeda, *RSC Adv.*, 2016, **6**, 74696–74699.
12 K. Sugikawa, K. Kozawa, M. Ueda and A. Ikeda, *Chem.–Eur. J.*, 2017, **23**, 13704–13710.
13 K. Sugikawa, Y. Inoue, K. Kozawa and A. Ikeda, *ChemNanoMat*, 2018, **4**, 682–687.
14 K. Sugikawa, A. Kubo and A. Ikeda, *Chem. Lett.*, 2016, **45**, 60–62.
15 Y. Doi, A. Ikeda, M. Akiyama, M. Nagano, T. Shigematsu, T. Ogawa, T. Takeya and T. Nagasaki, *Chem.–Eur. J.*, 2008, **14**, 8892–8897.
16 A. Ikeda, S. Hino, T. Mae, Y. Tsuchiya, K. Sugikawa, M. Tsukamoto, K. Yasuhara, H. Shigeto, H. Funabashi, A. Kuroda and M. Akiyama, *RSC Adv.*, 2015, **5**, 105279–105287.
17 Y. Tsuchiya, T. Shiraki, T. Matsumoto, K. Sugikawa, K. Sada, A. Yamano and S. Shinkai, *Chem.–Eur. J.*, 2012, **18**, 456–465.
18 T. Nakaya, B. Horiguchi, S. Hino, K. Sugikawa, H. Funabashi, A. Kuroda and A. Ikeda, *Photochem. Photobiol. Sci.*, 2019, **18**, 459–466.
19 R. G. Alargova, S. Deguchi and K. Tsujii, *J. Am. Chem. Soc.*, 2001, **123**, 10460–10467.

20 J. Brant, H. Lecoanet, M. Hotze and M. Wiesner, *Environ. Sci. Technol.*, 2005, **39**, 6343–6351.
21 K. Kano, R. Nishiyabu, T. Asada and Y. Kuroda, *J. Am. Chem. Soc.*, 2002, **124**, 9937–9944.
22 T. CaroFiglio, R. Fornasier, V. Lucchini, C. Rosso and U. Tonellato, *Tetrahedron Lett.*, 1996, **37**, 8019–8022.
23 A. Harada, *Coord. Chem. Rev.*, 1996, **148**, 115–133.
24 Y. Ishibashi, M. Arinishi, T. Katayama, H. Miyasaka and T. Asahi, *Chem. Lett.*, 2012, **41**, 1104–1106.
25 X. Chang and P. J. Vikesland, *Environ. Sci. Technol.*, 2011, **45**, 9967–9974.
26 C. S. Yannoni, R. D. Johnson, G. Meijer, D. S. Bethune and J. R. Salem, *J. Phys. Chem.*, 1991, **95**, 9–10.
27 D. Y. Sun, F. S. Tham, C. A. Reed, L. Chaker and P. D. W. Boyd, *J. Am. Chem. Soc.*, 2002, **124**, 6604–6612.
28 P. D. W. Boyd, M. C. Hodgson, C. E. F. Rickard, A. G. Oliver, L. Chaker, P. J. Brothers, R. D. Bolskar, F. S. Tham and C. A. Reed, *J. Am. Chem. Soc.*, 1999, **121**, 10487–10495.
29 B. A. Lindig, M. A. J. Rodgers and A. P. Schaap, *J. Am. Chem. Soc.*, 1980, **102**, 5590–5593.
30 I. Nakanishi, S. Fukuzumi, T. Konishi, K. Ohkubo, M. Fujitsuka, O. Ito and N. Miyata, *J. Phys. Chem. B*, 2002, **106**, 2372–2380.